

to glaciare at relatively warm temperatures in the presence of African dust (35), an effect that could alter cloud radiative processes, precipitation, and cloud lifetimes.

The great variability of African dust transport has broader implications beyond weather and climate. Iron associated with dust is an important micronutrient for phytoplankton (36). Thus, variations in dust transport to the oceans could modulate ocean primary productivity and, consequently, the ocean carbon cycle and atmospheric CO₂. Certain species of cyanobacteria also use iron in their metabolism; the rate of production of nitrate, a primary nutrient, by these organisms could be strongly influenced by dust inputs (36, 37).

Finally, during intense drought phases, the concentration of respirable dust (38) over the Caribbean probably exceeds the U.S. Environmental Protection Agency's 24-hour standard. Although there is no evidence that exposure to dust across this region presents a health problem, it does demonstrate how climate processes can bring about changes in our environment that could have a wide range of consequences on intercontinental scales.

References and Notes

1. Y. K. Kaufman, D. Tanré, O. Boucher, *Nature* **419**, 215 (2002).
2. Satellite images are available at <http://visibleearth.nasa.gov/Atmosphere/Aerosols>.
3. R. B. Husar, J. M. Prospero, L. L. Stowe, *J. Geophys. Res.* **102**, 16889 (1997).
4. J. T. Houghton et al., Eds., *Climate Change 2001: The Scientific Basis* (Contribution of Working Group I to the Third Assessment Report of the Intergovernmental Panel on Climate Change, Cambridge Univ. Press, New York, 2001).
5. J. M. Prospero, R. T. Nees, *Nature* **320**, 735 (1986).
6. X. Li, H. Maring, D. Savoie, K. Voss, J. M. Prospero, *Nature* **380**, 416 (1996).
7. J. M. Prospero, *J. Geophys. Res.* **104**, 15917 (1999).
8. Materials and methods are available as supporting material on Science Online.
9. K. D. Perry, T. A. Cahill, R. A. Eldred, D. D. Dutcher, T. E. Gill, *J. Geophys. Res.* **102**, 11225 (1997).
10. S. Nicholson, *Rev. Geophys.* **38**, 117 (2000).
11. P. J. Lamb, R. A. Pepler, *J. Clim.* **5**, 476 (1992).
12. J. M. Prospero, P. J. Lamb, unpublished data.
13. D. A. Gillette, *Cont. Atmos. Phys.* **72**, 67 (1999).
14. C. K. Folland, T. N. Palmer, D. E. Parker, *Nature* **320**, 602 (1986).
15. M. N. Ward, *J. Clim.* **11**, 3167 (1998).
16. C. Moulin, C. E. Lambert, F. Dulac, U. Dayan, *Nature* **387**, 691 (1997).
17. P. Ginoux, J. M. Prospero, O. Torres, M. Chin, *Environ. Modelling Software*, in press. DOI: 10.1016/S1364-8152(03)00114-2
18. G. N. Mbourou, J. J. Bertrand, S. E. Nicholson, *J. Appl. Meteorol.* **36**, 868 (1997).
19. J. M. Prospero, P. Ginoux, O. Torres, S. Nicholson, T. Gill, *Rev. Geophys.* **40**, 2, 10.1029/2000RG000095 (2002).
20. A. S. Goudie, N. J. Middleton, *Clim. Change* **20**, 197 (1992).
21. N. Brooks, M. Legrand, in *Linking Climate Change to Land Surface Change*, S. J. McLaren, D. R. Kniveton, Eds. (Kluwer, New York, 2000), pp. 1–25.
22. M. H. Glantz, Ed., in *Drought Follows the Plow: Cultivating Marginal Areas* (Cambridge Univ. Press, Cambridge, MA, 1994), pp. 33–43.
23. "Table HD.1 Demographic Indicators," World Resources Institute: Earth Trends (2001) (available at <http://earthtrends.wri.org/datatables/index.cfm?theme=4&CFID=225007&CFTOKEN=16244892>).
24. S. E. Nicholson, C. J. Tucker, M. B. Ba, *Bull. Am. Meteorol. Soc.* **79**, 815 (1998).
25. A. S. Goudie, N. J. Middleton, *Earth Sci. Rev.* **56**, 179 (2001).
26. P. Ginoux et al., *J. Geophys. Res.* **106**, 20255 (2001).
27. V. Ramaswamy et al., in (4), pp. 349–416.
28. J. Lelieveld et al., *Science* **298**, 794 (2002).
29. J. A. van Aardenne et al., *Global Biogeochem. Cycles* **15**, 909 (2001).
30. S. E. Nicholson, B. Some, B. Kone, *J. Clim.* **13**, 2628 (2000).
31. I. N. Sokolik et al., *J. Geophys. Res.* **106**, 18015 (2001).
32. J. P. Diaz et al., *J. Geophys. Res.* **106**, 18403 (2001).
33. C. W. Landsea, W. M. Gray, *J. Clim.* **5**, 435 (1992).
34. D. Rosenfeld, Y. Rudich, R. Lahav, *Proc. Nat. Acad. Sci. U.S.A.* **98**, 5975 (2001).
35. K. Sassen, P. J. DeMott, J. M. Prospero, M. R. Poellot, *Geophys. Res. Lett.* **30**, 1633, 10.1029/2003GL017371 (2003).
36. P. G. Falkowski, R. T. Barber, V. Smetacek, *Science* **281**, 200 (1998).
37. A. F. Michaels et al., *Biogeochemistry* **35**, 181 (1996).
38. J. M. Prospero, I. Olmez, M. Ames, *J. Water Air Soil Pollut.* **125**, 291 (2001).
39. The National Oceanic and Atmospheric Administration–Cooperative Institute for Research in Environmental Sciences (NOAA–CIRES) Climate Diagnostics Center Multivariate ENSO Index is available at www.cdc.noaa.gov/~kew/MEI/mei.html.
40. We thank H. Maring, D. Savoie, L. Custals, and T. Snowdon (University of Miami); C. Shea (Barbados); and D. Portis and I. Lele (University of Oklahoma) for technical support and E. Manning (Dyserth, North Wales, UK) and family for permitting us to operate our laboratory on their property in Barbados. Supported by grants from NSF, NASA, and NOAA.

Supporting Online Material

www.sciencemag.org/cgi/content/full/302/5647/1024/DC1

Materials and Methods

SOM Text

31 July 2003; accepted 9 October 2003

Oceanic Forcing of Sahel Rainfall on Interannual to Interdecadal Time Scales

A. Giannini,^{1*}† R. Saravanan,¹ P. Chang²

We present evidence, based on an ensemble of integrations with NSIPP1 (version 1 of the atmospheric general circulation model developed at NASA's Goddard Space Flight Center in the framework of the Seasonal-to-Interannual Prediction Project) forced only by the observed record of sea surface temperature from 1930 to 2000, to suggest that variability of rainfall in the Sahel results from the response of the African summer monsoon to oceanic forcing, amplified by land-atmosphere interaction. The recent drying trend in the semi-arid Sahel is attributed to warmer-than-average low-latitude waters around Africa, which, by favoring the establishment of deep convection over the ocean, weaken the continental convergence associated with the monsoon and engender widespread drought from Senegal to Ethiopia.

The cause of the persistence of drought in the African Sahel during the 1970s and 1980s (1) has yet to be determined. Is human activity to blame, or is climate variability an issue that the newly independent nations of sub-Saharan Africa would have to contend with as they devised strategies for their development (2)?

Over the past 30 years, research into the physical cause(s) of the recurrence of drought in Africa has progressed along two parallel directions. One, motivated by the belief that humanity was irreversibly impacting the environment and climate—by way of land cover and/or land use changes associated with the expansion of farming and herding into marginal areas, ultimately linked to the pressure of rapid population growth—emphasized

the role of the feedback between the atmospheric circulation and land surface processes. The other, revitalized by the initial successes in dynamical seasonal prediction of the mid-1980s, pointed to the atmospheric response to temperature changes in the global oceans as the leading cause of African climate variability.

Charney's influential work on the positive albedo-precipitation feedback (3, 4) pointed to the potential relevance of land surface conditions in the prolonged Sahel drought; an increase in surface albedo due to a human-induced change in vegetation cover could cause a decrease in precipitation that, in turn, would lead to a decrease in vegetation cover and thus a further enhancement of the albedo. What has become popularly known as "Charney's hypothesis" has, through the years, engendered a number of modeling studies of increasing detail (5–7). Although these studies generally support a land surface feedback mechanism, the extent to which this mechanism constitutes the leading cause of African climate variability has not been established, in part because the prescribed changes in land surface and/or vegetation cover were largely ex-

¹National Center for Atmospheric Research, Boulder, CO 80305, USA. ²Department of Oceanography, Texas A&M University, College Station, TX 77843, USA.

*To whom correspondence should be addressed. E-mail: alesall@iri.columbia.edu

†Present address: International Research Institute for Climate Prediction, Palisades, NY 10964, USA.

REPORTS

aggregated. In fact, the notion of the overpowering, destructive influence of human activity on a “pristine African environment” during the 20th century has recently been challenged (8–10). Using remotely sensed observations of vegetation, it had already been shown (11) that the latitudinal location of the Sahara-Sahel border is subject to fluctuations that can, in large part, be explained as the adjustment to interannual rainfall variability.

In the mid-1980s, modeling studies (12–14) spurred by advances in dynamical seasonal climate prediction confirmed the statistical association between observed Sahel rainfall variability and tropical Atlantic sea surface temperature (SST) (15, 16), for the first time suggesting a role for the other oceans as well. Hence, the focus progressively shifted away from the self-perpetuating role of desertification toward that of global oceanic conditions as the trigger for drought (17). However, success in modeling was limited to case studies, either forced with idealized SST anomalies obtained by compositing on the wettest and

driest Sahel years or aimed at reproducing the response in specific anomalous years. The extent to which global SSTs contribute to the long-term variability of Sahel precipitation has not, to date, been fully demonstrated.

The purpose of this report is to give a quantitative assessment of the importance of the oceanic influence on the variability of African climate on interannual to interdecadal time scales and to elucidate the associated dynamical processes. We analyze the variability of northern summer African monsoon precipitation in an ensemble of nine simulations spanning the 1930–2000 period (18). In the ensemble mean, any agreement with observed climate variability can only come from the observed SSTs imposed as the common oceanic boundary condition (19), because atmospheric CO₂ concentrations are held constant in time, at 350 parts per million, and vegetation cover is prescribed to vary seasonally but not interannually.

Figure 1 shows a comparison of long-term climate variability in the Sahel (10°N to 20°N, 20°W to 35°E) in observations (20) and in the

model. The correlation between the two time series of July to September (JAS) rainfall, characterized by a distinct negative trend between the wetter-than-average 1950s and the progressively drier decades of the 1960s, 1970s, and 1980s, is 0.60. The fact that the historical climatic progression can be reproduced using SST as the only external forcing demonstrates that the secular change in Sahel rainfall during the past century was not a direct consequence of regional environmental change, anthropogenic in nature or otherwise.

We further show that rainfall variability associated with the northern summer African monsoon is dominated by two distinct patterns that explain most of the rainfall variance (on the order of 40% in observations, 50% in the model’s ensemble mean). These patterns are well separated geographically, act on different time scales, and are linked to distinctively different patterns of SST. We obtained these patterns by applying principal component analysis (PCA) (21) and linear regression analysis to observed and modeled summer precipitation over tropical Africa (20°S to 20°N). Results are summarized in Fig. 2. The spatial patterns associated with the two leading principal components (PCs) of modeled precipitation (Fig. 2, A and D) highlight the separation between the oceanic Intertropical Convergence Zone (ITCZ) and its extension along the Gulf of Guinea coast, between the equator and 10°N, and continental convergence in the Sahel, between 10°N and 20°N. This separation is confirmed in observations (22). One PC is dominated by variability on the interannual time scale, whereas the other captures interdecadal variability (Fig. 2, B and E). In Fig. 2, C and F, contrast the localized to the eastern equatorial Atlantic character of the

Fig. 1. Indices of Sahel rainfall variability. Observations used the average of stations between 10°N and 20°N, 20°W and 40°E. Model numbers were based on the ensemble-mean average of grid-boxes between 10°N and 20°N, 20°W and 35°E. The correlation between observed and modeled indices of (JAS) rainfall over 1930–2000 is 0.60. (Time series are standardized to allow for an immediate comparison, because variability in the ensemble mean is muted in comparison to the single observed realization. The ratio of observed to ensemble-mean standard deviations in the Sahel is 4.)

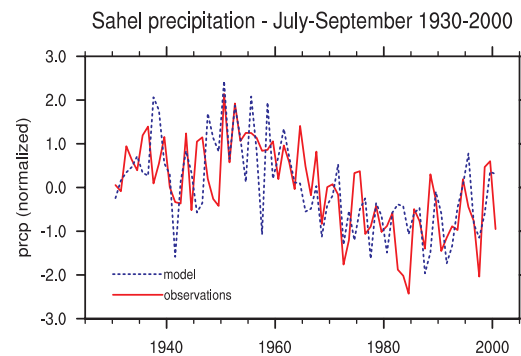
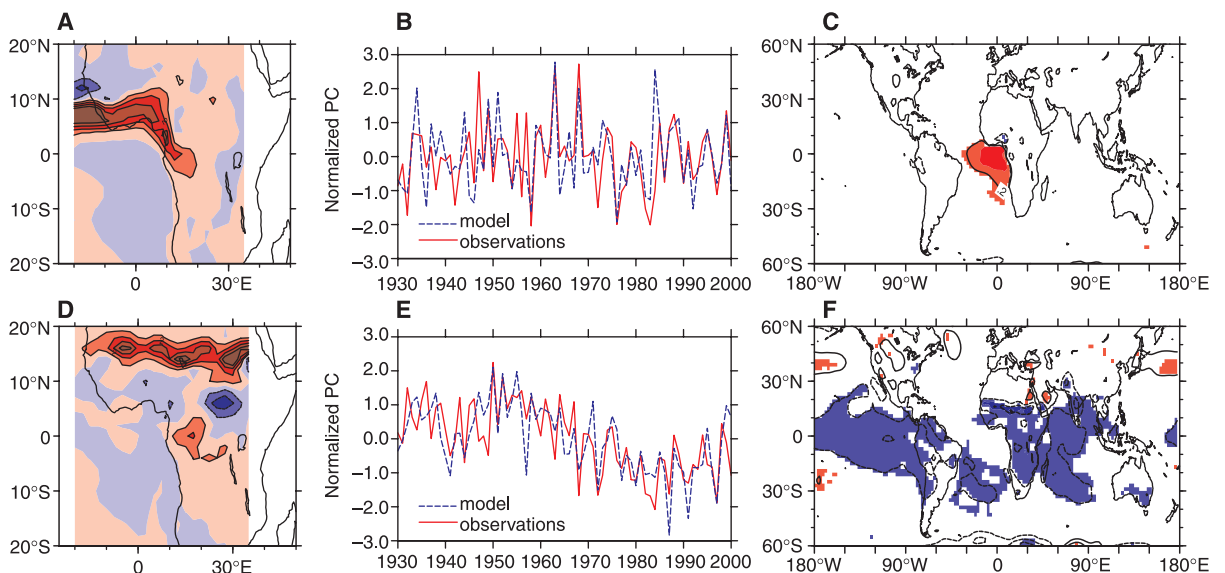


Fig. 2. Results of a PCA of northern summer rainfall over tropical Africa during 1930–2000. The two leading patterns of observed precipitation explain 25% and 15% of the total variance, their modeled counterparts 32% and 21% of the ensemble-mean variance, respectively. (A and D) Leading spatial patterns (EOFs) in the model. Red, positive precipitation anomalies; blue, negative anomalies. (B and E) Leading PCs; (B) is interannual in nature, whereas (E) captures the well-known trend in Sahel rainfall. The correlation between observed (red, solid line) and modeled (blue, dashed line) Gulf of Guinea PCs is 0.62; that between Sahel PCs is 0.73. (C and F) Regression maps of the leading model PCs with



ensemble-mean surface temperature. Contour interval is every 0.4 K, starting at 0.2 K, and shading represents statistical significance of the anomalies at the 99.9% level or higher. Solid lines and red color, positive anomalies; dashed lines and blue color, negative anomalies.

regression of the Gulf of Guinea PC with surface temperature (23) to the global character of the regression of the Sahel PC with surface temperature (over land it is the simulated, ensemble-mean surface temperature, whereas over the oceans it is the prescribed, observed SST).

A positive rainfall anomaly of one standard deviation in the Sahel PC (0.73 mm/day in observations) is associated with negative SST anomalies in the tropical Pacific and Indian Oceans of 0.2°C or larger and with negative surface temperature anomalies in the Sahel of up to 0.6°C (Fig. 2F). Over land, above average rainfall leads to above-average soil moisture. Because the incident energy flux is used preferentially to evaporate moisture rather than to heat the surface, enhanced precipitation over land goes together with increased soil moisture and evaporation and decreased land surface temperature. Consistent with this, the recent negative trend in Sahel rainfall was accompanied by an equally strong, positive surface temperature trend, simulated by

the model and confirmed in observations (22).

In the presence of a positive precipitation anomaly, the enhanced upward motion that characterizes deep convection is accompanied by enhanced mid-level condensation and latent heat release, which further fuel rising motion and large-scale moisture convergence (24). Increased evaporation also contributes to this positive dynamical feedback, by locally recycling moisture. The evaporation anomaly accounts for one-third of the precipitation anomaly, whereas the larger part is contributed by moisture convergence (22).

Thus a land-atmosphere feedback acts to amplify the ocean-forced precipitation signal. To compare the relative impacts of oceanic forcing and land-atmosphere interaction on Sahel rainfall, we analyzed two additional integrations in which either interannual SST variability or land-atmosphere interaction were disabled (25). We compared Sahel rainfall variability by projecting the pattern in Fig. 2D onto the precipitation fields taken from these additional integrations. Results are shown in Fig. 3. In the absence of

interannual SST variability (Fig. 3A), variability in the Sahel is muted: the variance in Sahel precipitation is reduced to one-quarter of that in the ensemble mean. In the absence of land-atmosphere interaction (Fig. 3B), the long-term variability of Sahel rainfall is still successfully reproduced (the correlation with the ensemble-mean time series over 1950–1999 is 0.83), but variance is also consistently weaker (by 40%) than in the ensemble mean. This comparison supports the conclusion that SST variability is instrumental in determining the sign of rainfall anomalies in the Sahel, whereas coherent land-atmosphere interaction acts to amplify them (26).

In order to identify the causes of the trend in Sahel rainfall, we decomposed the Sahel PC into high- and low-frequency components (27) (Fig. 4). “Low-frequency” here is defined as the result of a 21-year running mean of the PC, whereas “high-frequency” is its residual. This decomposition highlights the role of the slower oceanic variability characteristic of the southern Atlantic and Indian Oceans in forcing the trend (Fig. 4, B

Fig. 3. Projection of the ensemble-mean Sahel EOF onto precipitation in two additional integrations. (A) When interannual SST variability is disabled, variability in precipitation is reduced. (B) When land-atmosphere interaction is disabled, decadal variability is still adequately reproduced. All time series are normalized by the square root of the eigenvalue associated with the ensemble-mean Sahel EOF. AMIP, Atmospheric Model Intercomparison Project.

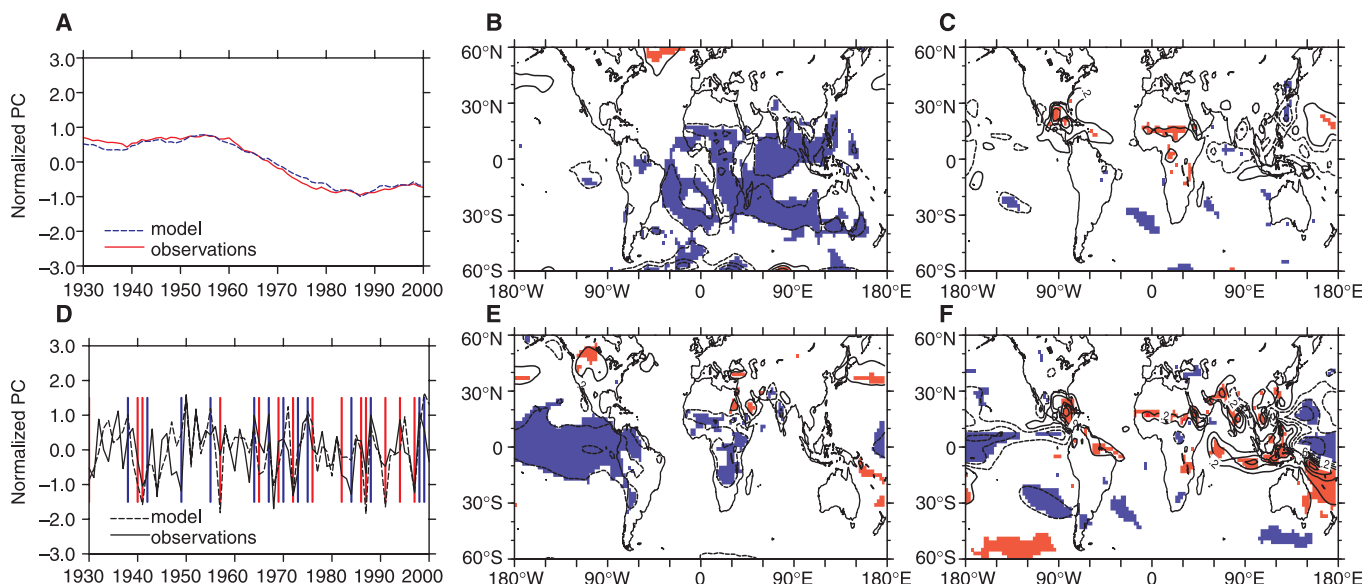
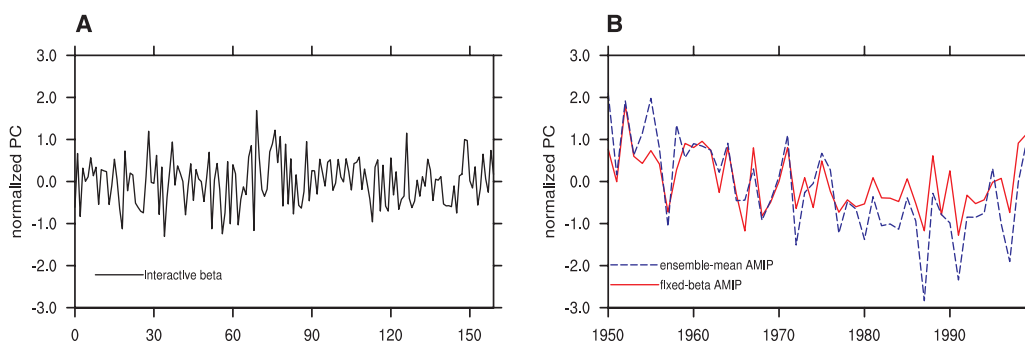


Fig. 4. Decomposition of the Sahel PC of precipitation into low (A to C) and high frequency (D to F) components. (A) Twenty-one year running mean of the Sahel PC, in observations (red), and in the model (blue). (D) Solid lines, the observed PC; dashed lines, the modeled PC. Correlation is 0.52, meaning that the success of the simulations comes from their ability to capture more than just the interdecadal variability. The ver-

tical lines represent ENSO events: warm in red, cold in blue. (B and E) Regression maps of the (B) low- and (E) high-frequency components of the Sahel PC with ensemble-mean surface temperature. Contouring and shading are as in Fig. 2. [(C) and (F)] Regression maps with precipitation. Contour interval is every 0.4 mm/day, starting at 0.2 mm/day.

and C), while confining the influence of the El Niño-Southern Oscillation (ENSO) (28, 29) to the interannual time scale (Fig. 4, E and F).

The semi-arid Sahel emerges as a region highly sensitive to SST variability in all tropical basins, remote (Pacific) and local (Atlantic and Indian). A positive trend in equatorial Indian Ocean SSTs, between East Africa and Indonesia, is identified as the proximate cause for the negative rainfall trend observed in the Sahel from the late 1960s to the 1980s (Fig. 4, A and B). Teaming up with an occasionally warmer-than-average eastern equatorial Atlantic Ocean (15, 16), it formed a low-latitude ring of warm SSTs around Africa that may have disrupted the fragile balance that defines the monsoon, between the competing effects of high summertime land surface temperatures and the associated development of a land-ocean temperature contrast versus the availability of moisture (30). Rainfall anomalies of opposite sign across the Sahel and in the equatorial Indian Ocean (Fig. 4C) support the hypothesis that the oceanic warming around Africa may indeed have weakened the land-ocean temperature contrast and consequently the monsoon, causing deep convection to migrate over the ocean and engendering widespread drought over land, from the Atlantic coast of West Africa to the highlands of Ethiopia.

References and Notes

1. S. E. Nicholson, *Mon. Weather Rev.* **108**, 473 (1980).
2. M. H. Glantz, R. W. Katz, *Ambio* **14** (no. 6), 334 (1985).
3. J. G. Charney, *Q. J. R. Meteorol. Soc.* **101**, 193 (1975).
4. The albedo-precipitation feedback popularized by Charney was first proposed by J. Otterman [*Science* **186**, 531 (1974)].
5. Y. C. Sud, M. Fennessy, *J. Clim.* **2**, 105 (1982).
6. Y. Xue, J. Shukla, *J. Clim.* **6**, 2232 (1993).
7. C. M. Taylor, E. F. Lambin, N. Stephenne, R. J. Harding, R. L. H. Essery, *J. Clim.* **15**, 3615 (2002).
8. J. Fairhead, M. Leach, *Deforestation: Global analyses and local realities — studies in West Africa* (Routledge, London, 1998).
9. E. F. Lambin et al., *Global Environ. Change* **11**, 261 (2001).
10. K. Rasmussen et al., *Global Environ. Change* **11**, 271 (2001).
11. C. J. Tucker, H. E. Dregne, W. W. Newcomb, *Science* **253**, 299 (1991).
12. C. K. Folland, T. N. Palmer, D. E. Parker, *Nature* **320**, 602 (1986).
13. T. N. Palmer, *Nature* **322**, 251 (1986).
14. D. P. Rowell, C. K. Folland, K. Maskell, M. N. Ward, *Q. J. R. Meteorol. Soc.* **121**, 669 (1995).
15. S. Hastenrath, P. J. Lamb, *Mon. Weather Rev.* **105**, 1019 (1977).
16. P. J. Lamb, *Mon. Weather Rev.* **106**, 482 (1978).
17. B. Fontaine, S. Janicot, *J. Clim.* **9**, 2935 (1996).
18. NSIPP1, as described in abstract. J. T. Bacmeister, P. J. Pegion, S. D. Schubert, M. J. Suarez, *NASA Technical Memo. 104606*, vol. 17 (2000). Available at <http://nsipp.gsfc.nasa.gov>.
19. SSTs from three different data sets were used to force the ensemble of atmospheric general circulation model (AGCM) integrations over the sub-periods 1930–48, 1949–81, and 1982–2000. The data sets are (i) the Hadley Centre product (37), (ii) the GISST product (32), and (iii) the “Reynolds” product (33). The temporal discontinuities in boundary conditions were found to be of no consequence to the analysis presented here: the regression pattern of Fig. 2F was recalculated using the Hadley Centre data set from 1930 to 1999 and found to be identical to the one presented here, calculated using the boundary condition data set. Also, projections of the same regression pattern onto the Hadley Centre prod-

uct and onto the boundary condition data set were found to correlate at 0.97 when care was taken to exclude gridpoints south of 50°S.

20. R. S. Vose et al., *The Global Historical Climatology Network: Long-term monthly temperature, precipitation, sea level pressure, and station pressure data*. ORNL/CDIAC-53, NDP-041 (Carbon Dioxide Information Analysis Center, Oak Ridge National Laboratory, Oak Ridge, TN, 1992).
21. PCA is a mathematical procedure routinely used in the geophysical sciences to extract the dominant patterns of variability. It identifies the spatial structures, or empirical orthogonal functions (EOFs), and related temporal structures, also known as PCs, that sequentially maximize the fraction of the total variability that they represent (34–36).
22. A. Giannini, R. Saravanan, P. Chang, data not shown.
23. The impact of tropical Atlantic SST anomalies on the West African monsoon has been the subject of observational studies dating back to the 1970s (15, 16), as well as of two recent modeling studies by Vigny and Cook (37, 38). In the presence of an equatorial Atlantic SST anomaly akin to the one associated with the model’s Gulf of Guinea PC (Fig. 2C), a dipole in precipitation stands out in observations, with anomalies of opposite sign in the Sahel and along the Gulf of Guinea coast. This dipole is captured in our analysis of observed rainfall variability in the Sahel EOF (22); the regression of the observed Sahel PC onto SST (22) does bear the association out, with significant regression anomalies in the equatorial Atlantic, as well as in the rest of the tropical oceans. PCA of model output, in contrast, though separating rainfall variability in the Sahel from rainfall variability along the Gulf of Guinea coast (Fig. 2, A and D) in the two leading EOFs also decouples the association between eastern equatorial Atlantic SSTs and the rainfall dipole. AGCMs, thus far, have not been able to capture the dipole in precipitation, and the model analyzed here is no exception. Whether this model’s failure to explicitly represent the dipole in precipitation is a dynamical limitation of the model, an artifact of PCA, or the expression of a substantial dynamical difference between Sahel and Gulf of Guinea precipitation, remains to be seen.
24. K. H. Cook, *J. Clim.* **7**, 400 (1994).
25. Interannual SST variability is disabled in a 160-year long integration by substituting the observed record of SST with monthly climatology. Land-atmosphere interaction is disabled in a single integration forced with the observed record of SST over 1950–1999 by fixing evaporation efficiencies to monthly climatology, as computed from the ensemble of integrations. For details on the method, see (39, 40).

26. An interactive vegetation, in addition to the interactive land surface, could further amplify the ocean-forced signal, as in the intermediate complexity model of N. Zeng, J. D. Neelin, K.-M. Lau and C. J. Tucker [*Science* **286**, 1537 (1999)]. Such an amplification could at least partially account for the difference in magnitude between observed and modeled rainfall variability (Fig. 1).
27. M. N. Ward, *J. Clim.* **11**, 3167 (1998).
28. S. Janicot, A. Harzallah, B. Fontaine, V. Moron, *J. Clim.* **11**, 1874 (1998).
29. J. C. H. Chiang, A. H. Sobel, *J. Clim.* **15**, 2616 (2002).
30. C. Chou, J. D. Neelin, H. Su, *Q. J. R. Meteorol. Soc.* **127**, 1869 (2001).
31. N. A. Rayner et al., in press.
32. N. A. Rayner, E. B. Horton, D. E. Parker, C. K. Folland, R. B. Hackett, *Climate Research Technical Note 74* (1996). Available at: www.met-office.gov.uk/research/hadleycentre/obsdata/GISST.html
33. W. R. Reynolds, T. M. Smith, *J. Clim.* **7**, 929 (1994).
34. R. W. Preisendorfer, *Principal Component Analysis in Meteorology and Oceanography*, C. Mobley, Ed. (Elsevier, Amsterdam, 1988).
35. H. von Storch, F. W. Zwiers, *Statistical Analysis in Climate Research* (Cambridge Univ. Press, Cambridge, 1999).
36. J. P. Peixoto, A. H. Oort, *Physics of Climate* (American Institute of Physics, New York, 1992), appendix B.
37. E. K. Vizy, K. H. Cook, *J. Clim.* **14**, 795 (2001).
38. E. K. Vizy, K. H. Cook, *J. Geophys. Res.* **107**(D3), doi: 10.1029/2001JD000686 (2002).
39. R. D. Koster, M. J. Suarez, *J. Geophys. Res.* **100**(D7), 13775 (1995).
40. R. D. Koster, M. J. Suarez, M. Heiser, *J. Hydrometeorol.* **1**, 26 (2000).
41. We acknowledge the scientific advice and technical support provided by M. Suarez and the NSIPP Team at NASA/GSFC (M. Rienecker, J. Bacmeister, M. Kistler, S. Schubert, P. Pegion, and N. Johnson). Supported in part by NASA InterAgency agreement W-19,750. The National Center for Atmospheric Research is operated by the University Corporation for Atmospheric Research under sponsorship of NSF.

18 July 2003; accepted 26 September 2003
 Published online 9 October 2003;
 10.1126/science.1089357
 Include this information when citing this paper.

Increased Longevities of Post-Paleozoic Marine Genera After Mass Extinctions

Arnold I. Miller^{1*} and Michael Foote²

Cohorts of marine taxa that originated during recoveries from mass extinctions were commonly more widespread spatially than those originating at other times. Coupled with the recognition of a correlation between the geographic ranges and temporal longevities of marine taxa, this observation predicts that recovery taxa were unusually long-lived geologically. We analyzed this possibility by assessing the longevities of marine genus cohorts that originated in successive substages throughout the Phanerozoic. Results confirm that several mass extinction recovery cohorts were significantly longer lived than other cohorts, but this effect was limited to the post-Paleozoic, suggesting differences in the dynamics of Paleozoic versus post-Paleozoic diversification.

In evaluating the global biotic effects of mass extinctions, attention has focused increasingly on recovery biotas, the taxa that originated or contributed to diversity in the immediate aftermaths of extinction events (1–5). Postextinction diver-

sification has proven to be more geographically and temporally complex than once envisioned, with the onset of major rebounds in diversity characterized by lag times and geographic variability (6–9). Nevertheless, several principles